Arabian Journal of Chemistry (2023) **16**, 104412

King Saud University

Arabian Journal of Chemistry

www.ksu.edu.sa
www.sciencedirect.com

ORIGINAL ARTICLE

Preparation of carbon-aerogel polypyrrole composite for desalination by hybrid capacitive desalination method

Michael Beke, Tarisai Velempini, Eswaran Prabakaran, Kriveshini Pillay *

Department of Chemical Sciences, University of Johannesburg, South Africa

Received 4 February 2022; accepted 7 November 2022
Available online 12 November 2022

KEYWORDS

Carbon aerogel;
Polypyrrole composite;
Capacitive Deionization;
Desalination

Abstract Capacitive Deionization (CDI) is an emerging technology with great potential applications. Most researchers view it as a viable water treatment alternative to reverse osmosis. This research reports the preparation and application of a carbon aerogel polypyrrole (CA-PPy) composite for the desalination of NaCl solution by the hybrid CDI method. The carbon aerogel (CA) was prepared from a Resorcinol / Formaldehyde precursor by the sol–gel method. The aerogel obtained from the sol–gel was then pyrolysed in a tube furnace to form CA. Polypyrrole (PPy) was prepared by the Oxidative chemical polymerisation of pyrrole, ferric chloride hexahydrate (oxidant), and sodium dodecyl sulfate (dopant). A composite of CA and PPy was then prepared and used to modify carbon electrodes. The CA-PPy composite was characterised to verify its composition, morphology, thermal properties, and functional groups. The electrochemical properties of the material were determined by Cyclic voltammetry (CV) and Electrochemical impedance spectroscopy (EIS) tests. The electrochemical tests were done using a GAMRY potentiostat electrochemical workstation, a 1.0 M KCl was used as the electrolyte, and the applied potential window was (-0.2 to + 0.6) V for the CV test. The EIS test was done with the same concentration of KCl electrolyte at an applied potential of 0.22 V and at a frequency range of (0.1 – 100, 000) Hz. The optimal specific capacitance of the CA is 115F/g, and that of the composite is 360.1F/g, they were both obtained at a scan rate of 5 mV/s. The CDI desalination study of the CA-PPy composite showed a salt adsorption capacity (SAC) of 10.10 mg/g (300 mg/L NaCl solution) – 15.7 mg/g (800 mg/L NaCl solution) at 1.2 V applied voltage. The salt recovery efficiency of the electrode material in the 300 mg/L solution is 27 %, in the 500 mg/L solution, it is 20.12 %, and in the

* Corresponding author.
E-mail address: kriveshinip@uj.ac.z (K. Pillay).
Peer review under responsibility of King Saud University.

Production and hosting by Elsevier

https://doi.org/10.1016/j.arabjc.2022.104412

800 mg/L solution, it is 15.41 %. The electrode material also showed good electrochemical stability after nine cycles of ion adsorption/desorption study.

1. Introduction

Availability of consumable water is a major global challenge; hence there is a continuous scientific search to develop cost-effective and efficient technologies to convert the globally abundant volume of brackish water into consumable water (Laxman and Myint, 2015; Torres Hernández, 2018). Desalination literally means the removal of salt. Brackish and seawater have dissolved salts. The desalination technologies used to produce freshwater from brackish and seawater are thermal methods, electrodialysis (ED), and Reverse Osmosis (RO) (Khawaji et al., 2008; Burn et al., 2015). Whereas these methods of desalination are effective in the production of freshwater from saline water, they have peculiar and general challenges, ranging from high energy consumption to fouling of their membranes/electrodes (Burn et al., 2015). The cost of producing freshwater by these methods is relatively high, thermal methods are the most expensive followed ED method. RO method is cheaper than thermal and ED methods (Al-Karaghouli and Kazmerski, 2013), but the total energy consumption to produce freshwater by the RO method is still higher than that of the capacitive deionisation (CDI) method (Tan et al., 2022). RO is an established method of freshwater production by desalination, but CDI is considered a viable alternative method of freshwater production by desalination because of its cheaper cost of freshwater production (Qin et al., 2019). Capacitive deionisation is an emerging desalination technology that is cost-effective and efficient for freshwater production by desalination (Fahmida and Sultana, 2018; Hu et al., 2016). The operating principle of CDI systems can be described with the Gouy-Chapman-Stern electrical double layer (EDL) model. The mechanism of ion removal could be Faradic or non-Faradic depending on the type of electrodes used (Jia and Zhang, 2016; Oyarzun et al., 2018). The type of electrode material and its electrochemical features are paramount in the effectiveness and general performance of the CDI system; hence research in this field is focused on developing electrode materials with a high ion adsorption/desorption capacity, low cost, and electrochemical stability during CDI operations (Choi, 2014; Duan et al., 2015; Pera-Titus et al., 2020). For decades, different porous carbon materials were used for CDI studies. They have a large specific surface area and are electrically conductive (Rambabu et al., 2020). Some of the forms these carbon electrodes are utilised are carbon aerogels (Kumar et al., 2016), mesoporous Carbon (Zhang et al., 2013), activated carbon (Chen et al., 2018), carbon nanofibers (Oladunni et al., 2018), carbon nanotubes (Volfkovich, 2020), graphene (Liu et al., 2017), and carbon cloth (Oh et al., 2006). Carbon aerogel is one of the carbon materials of interest in CDI studies because it has a large specific surface area of (400 – 1100) m^2/g. Good electrical conductivity, low resistivity (about 400 Ωm/cm), and is thermally stable in aqueous solutions. Its micro and mesoporosity are tunable (Haro et al., 2011; Pekala, 1989). A stand-out property of CA as a CDI electrode is its interconnected particles with spaces in-between; this allows for ion storage (Li et al., 2012; Xia et al., 2012). A resorcinol and formaldehyde (RF) mixture may be used as precursors in the preparation of CA. The required morphology is achieved by adjusting the pH, catalyst concentration, and pyrolysis temperature (Al-Muhtaseb and Ritter, 2003; Xu et al., 2012). The ion adsorption capacity of CA may be enhanced by incorporating other materials (Conductive polymer) or metal oxide with CA to form a composite (Cheng et al., 2019; Porada et al., 2013). Zhang et al. reported the application of a graphene-carbon aerogel composite for CDI desalination studies; they reported an ion adsorption of 26.9 mg/g at a concentration of 500 mg/L of NaCl solution (Cao et al., 2019b). Carbon-aerogel composites have also been applied to remove heavy ions from wastewater by the CDI method (Cao et al., 2019a; Meena et al., 2005).

Most carbon materials have one or more of the following disadvantages, poor wettability, High production cost, and Low ion adsorption capacity. To circumvent these challenges, carbon materials are modified with materials with a high specific capacitance (Yang et al., 2011), such as conductive polymers like polypyrrole (PPy), polyaniline (PANI), and polythiophene (PTP) (Kumar et al., 2012; Wang et al., 2010; Zhang et al., 2013). CDI systems with such modified carbon electrodes are called HYBRID CDI cells. The modifier materials improve the performance of the carbon composite in the CDI system by tailoring the surface morphology, wettability, porosity, and electrical conductivity (Bose et al., 2011; Razaq et al., 2012). For example, Samanci et al., prepared a carbon-aerogel polypyrrole (CA-PPy) composite electrode for energy storage studies. An increase in specific capacitance from 147F/g for CA to 234F/g for the CA-PPy composite was reported (Samancı et al., 2021). The addition of PPy significantly improved the specific capacitance of the CA in the composite. Also, Zhuo et al., prepared CA from a cellulose material and modified it with PPy (Li et al., 2019a). The cellulose CA-PPy composite was studied as a supercapacitor material. They reported a high specific capacitance of 345F/g with capacitance retention of 92.6 % after 10,000 cycles. The research of Zhuo H. et al. and Samanci M. et al. cited above strongly implies that a CA-PPy composite will be an excellent material for hybrid CDI desalination. The aims of this study are to prepare a CA-PPy composite electrode material, investigate its physical and electrochemical properties, and apply it for the desalination of NaCl solution by the CDI method. To the best of our knowledge, the application of CA-PPy for desalination study is novel. Although the material has been previously prepared and studied as a supercapacitor material, we are not aware of its application for desalination studies by the hybrid CDI method.

2. Materials and method

2.1. Materials

Pyrrole (C_4H_4NH), ferric chloride hexahydrate ($FeCl_3[H_2O]_6$), ammonium persulphate ($(NH_4)_2S_2O_8$), sodium dodecyl-sulphate ($NaC_{12}H_{25}SO_4$), deionised water (H_2O), resorcinol ($C_6H_6O_2$), formaldehyde (CH_2O), hydrochloric acid (HCl), acetonitrile(C_2H_3N), and sodium chloride (NaCl), Polyvinylidene fluoride (-($C_2H_2F_2$)n-), *N*-methyl-pyrrolidone (C_5H_9NO), acetylene black (C), and Dimethyl-formamide (C_3H_7NO) were purchased from Sigma Aldrich, South Africa. All chemicals were used as received from the vendor.

2.2. Synthesis of polypyrrole (PPy)

Polypyrrole (PPy) was prepared by a chemical oxidation polymerisation method (Chitte et al., 2011). Ferric chloride was used as an oxidant, while sodium dodecyl sulphate was a dopant. 3.48 g of sodium dodecyl sulphate was dissolved in 100 mL of deionised water, 27.03 g of ferric chloride hexahydrate was also dissolved separately in 100 mL of deionised

water. The two solutions were mixed in a 500 mL beaker and stirred for 15 min. 0.15 mol of pyrrole was then gradually added into the mixture dropwise and stirred for 4 hrs. A black precipitate of PPy was formed and filtered off. The PPy was then washed several times with deionised water and later dried in an oven for 12 hrs. at 60 °C. The synthesis procedure of PPy was as shown in Scheme 1.

2.3. Synthesis of carbon aerogel (CA)

Aerogel was first synthesised by the sol–gel condensation of formaldehyde and resorcinol. 0.337 g of resorcinol was dissolved in 11.5 mL of acetonitrile, 0.477 mL of formaldehyde was added, followed by 0.09 mL of a concentrated hydrochloric acid catalyst; the mixture was then stirred for 5 min. The resultant solution was then transferred into 50 mL centrifuge tubes and left to age for three days. The resultant sol–gel was frozen to −80 °C before freeze drying to form the aerogel. The aerogel was then carbonised in a tube furnace at 600 °C for 4 hrs. under nitrogen gas flow to give a carbon aerogel (Xu et al., 2012; Tannert). The schematics of the preparation of CA is shown in Scheme 2.

2.4. Preparation of CA-PPy composite slurry

The CA and PPy were homogenised to form a CA-PPy composite slurry using a method that has been previously reported (Yong-Jin Han et al., 2011). 4.0 g of PPy and 8.0 g of CA were thoroughly mixed. 8.0 g of the CA-PPy mixture, 1.0 g of Polyvinylidene fluoride (PVDF as a binder), and 1.0 g of carbon black (conductive material) mixture were then dissolved in a 100 mL *N*-methyl pyrrolidone (NMP) solution, and the mix-

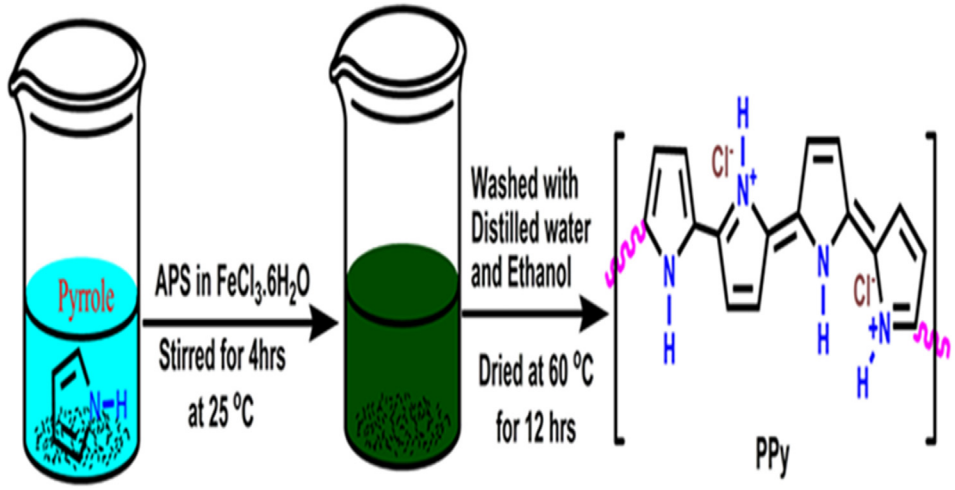

Scheme 1 Schematic of the Synthesis of Polypyrrole by Oxidative Polymerisation.

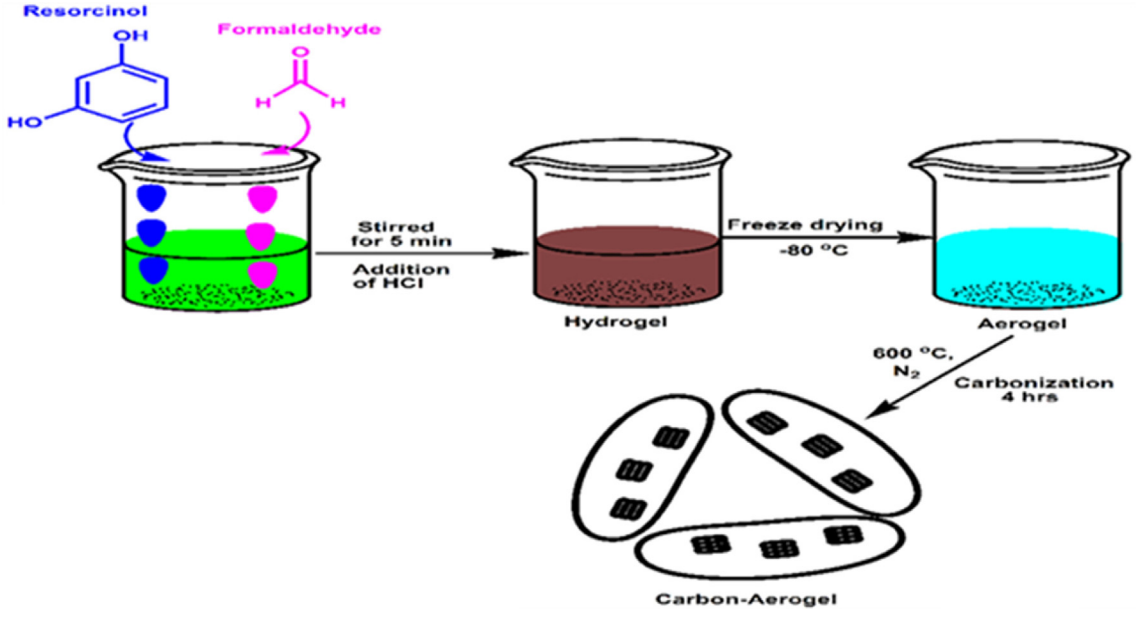

Scheme 2 Schematic of carbon aerogel synthesis by the sol–gel condensation method.

ture was stirred for 24 hrs to obtain a homogenous CA-PPy composite slurry. The ratio of the materials used to prepare the slurry is the standard adopted by most researchers (Rambabu et al., 2020; Zhao et al., 2017).

2.5. Coating of electrodes with CA-PPy composite slurry

The homogenised CA-PPy composite slurry was coated on activated carbon (AC) by the doctor blade drop coating method (Buczek et al., 2020). AC materials of 0.5 cm by 1.0 cm were first thoroughly washed in ethanol to remove any impurities. These were then dried in an oven at 80 °C for two hours, and the weights of the electrodes were then determined with a chemical balance. The CA-PPy composite slurry was then coated on the AC by the doctor blade drop coating method, it was then dried in a vacuum oven for 12 hrs at 100 °C. The weights of the modified electrodes are then determined on a chemical balance in anticipation to calculate the mass of CA-PPy composite on each of the AC electrodes. These were then applied as modified electrodes for desalination studies by the CDI method.

3. Characterisations of materials

Samples of the materials prepared were analysed on a Fourier Transform Infrared (FTIR) Spectroscopy (Spectrum-100 Perkin Elmer, USA). The FTIR analysis was carried out in the wavenumber range of 4000 to 500 cm^{-1}. X-ray diffraction (XRD) patterns were obtained on a Rigaku Ultima IV X-ray diffractometer, employing CuKα radiation at a wavelength of 1.5406 Å (generated at 45 kV and 40 mA). XRD patterns were collected in the 2θ range between 5° and 90° with a step size of 0.01°, and a scan speed of 1°/min. The morphologies of the samples were determined using scanning electron microscopy (SEM) (TESCAN, VEGA SEM, Czech Republic) at a 20 kV electron acceleration voltage. Energy Dispersive X-ray Spectroscopy (EDAX) was also employed to determine the prepared materials' homogeneity, elemental composition, and distribution. The surfaces of the samples were coated with carbon to avoid charging. The samples were dispersed in ethanol and sonicated for 5 min for TEM analysis. After dispersion, a mixture was drop-casted on a carbon-coated copper grid and dried for a while before analysis using the JEOL-2100 electron microscope. A JEOL-2100 transmission electron microscope operated at an acceleration voltage of 200 kV was used to reveal the internal structure of the materials. Raman spectroscopy was carried out with a Jobin-Yvon T64000 Raman Spectrometer coupled to an Argon ion pulsed laser as an excitation source with excitation taking place at a wavelength of 514 nm and a power of 21 mW. The materials' specific surface area (SSS) and porosity analysis were done with a (TriStar 3000, Micromeritics Instruments Corporation, Norcross, GA, USA.) N_2 adsorption/desorption equipment. The materials' SSS was determined from the adsorption isotherms using the Brunauer-Emmett-Teller (BET) calculations. The materials' thermal stability and combustion analysis were measured using a thermogravimetric analyser (TGA) instrument (GA; STA449C; Netzsch, Germany). The heating was done in a nitrogen gas atmosphere with the samples in a ceramic crucible; the heat rate was 20 °C/min.

3.1. Electrochemical characterisation

The electrochemical characterisations, include cyclic voltammetry (CV) and electrochemical impedance spectroscopy (EIS). Cyclic CV is an electrochemical method used to measure the current that is generated in an electrochemical cell under conditions where the applied voltage exceeds that predicted by the Nernst equation. CV tests are done by cycling the potential of a WE and measuring the resultant current. It is used to determine the oxidative and reductive properties of chemical substances. EIS is a very sensitive characterization method applied to establish an electrical response from chemical systems in a non-destructive manner. It investigates the response time of chemical systems using low amplitude alternating current (AC) voltages within a range of frequencies. A three-electrode system consisting of a working electrode (WE), reference electrode (RE), and a counter electrode (CE) was adopted for this study. A defined voltage was passed from the WE through an electrolytic solution and into the CE. This allows for a quantitative evaluation of small-scale chemical mechanisms at the electrode interface and within the electrolytic solution. The CV and EIS tests were done using a three-electrode Gamry potentiostat electrochemical workstation. The working electrode was an activated carbon sheet coated with the active material. A platinum wire was used as the counter electrode, and the reference electrode was an Ag-AgCl electrode. The electrolyte used for each experiment was a 1.0 M KCl solution. The potential window applied was −0.2 to + 0.6 V. The CV was done at different scan rates ranging from (5 to 100) mV/s. Electrochemical Impedance Spectra (EIS) was conducted over a frequency range of 0.1 Hz to 100 000 Hz. The applied potential for the EIS test is 0.22 V.

The specific capacitance (C_s) of the materials was evaluated from data of the CV experiment using Eq. (1) (Rambabu et al., 2020; O. logo et al., 2017)

$$C_s = \frac{\int idv}{2 * m * \Delta V * s} \quad (1)$$

Where the integral ($\int$idv) is the area of the CV spectra, m is the mass of CA-PPy (g), ΔV is the potential window (V), and S is the scan rate (mVs^{-1}).

3.2. CDI experiment for ion adsorption studies

The ion adsorption performance of the CA-PPy composite was conducted in the laboratory by the CDI method. Two AC electrodes of 0.5 cm by 1.0 cm were used as a cathode and anode, respectively. The anode was previously modified with the CA-PPy composite. These electrodes were then separated with a polythene material at a distance of 1.0 cm apart in a 100 mL beaker. 50 mL of NaCl solution was then transferred into the beaker (300 mg/L, 500 mg/L and 800 mg/L were used separately). An electrical conductivity meter was used to measure the conductance of the electrolyte throughout the experiment while it was constantly stirred with a magnetic stirrer at a speed of 200 rpm. The electrodes were then connected to a DC power source, and a potential of 1.2 V was applied.

On application of the potential, one of the electrodes becomes the cathode and the other the anode. The resultant polarization causes the cations Na^+ and anions Cl^- to migrate to the cathode and anode. The ions were adsorbed on the

surface of the electrodes. The process was allowed to continue until the electrodes were wholly loaded with ions (saturation). The electrodes were then transferred into another beaker containing deionised water, and the polarity at the electrodes was reversed for desorption to occur. This process was repeated several times, and the adsorption capacity and recyclability of the electrodes were monitored. The salt electrosorption capacity (A) of the electrodes was calculated using Eq. (2) (Alaei Shahmirzadi et al., 2018)

$$A = \frac{\Delta C * V(L)}{m} \tag{2}$$

Where ΔC = Change in concentration (mg/L), V = volume of NaCl solution used (L), m = mass of composite material on AC electrode (g).

The salt recovery efficiency (SRE) of the electrode material was also determined using methods previously reported. It was measured from the desalination conductivity data of the different concentrations of the NaCl solutions used for the study. Eq. (3) displays the formula used to determine the SRE (%).

$$SRE(\%) = \frac{\mathrm{Co} - C}{\mathrm{Co}} * 100 \tag{3}$$

Where Co = Initial conductivity of the solution, C = Final conductivity of the solution.

4. Results and discussion

4.1. Instrument details

4.1.1. FT-IR characterisation

Figure 1 (a-d) shows the FT-IR spectra of the carbon aerogel, CA (Fig. 1a), PPy (Fig. 1b), and CA-PPy (Fig. 1 c and d) in evaluating functional groups. CA displayed several peaks at 3380 cm^{-1}, 2852 cm^{-1}, 2539 cm^{-1}, 2185 cm^{-1}, 2006 cm^{-1}, 1580 cm^{-1}, 1177 cm^{-1} and 788 cm^{-1} which corresponds to stretching vibration of O—H, $=CH_2$, $\equiv$CH, aromatic C—H, —C$\equiv$C—, C$=$C, C—O—C, and C$=CH_2$ groups as shown in Fig. 1(a), and confirms the formation of the carbon aerogel after calcination (Heslop, 2007; Kobayashi and Konishi, 2009; Mahani et al., 2018; Wang et al., 2015) shows the spectrum of PPy. The spectrum of PPy showed various peaks at (1513 cm^{-1}, 1325 cm^{-1}), (1154 cm^{-1}, 1049 cm^{-1}) and 809 cm^{-1} which was attributed to the bending vibration of C$=$C, C—N, C—H and stretching C$=CH_2$ of the PPy ring (Alaei Shahmirzadi et al., 2018; Li et al., 2018; Wang et al., 2018). The 3382 cm^{-1} and 2874 cm^{-1} peaks were assigned to the stretching vibration of N—H and C-H_2 bonds (Oh et al., 2006; Ryoo et al., 2003). The CA-PPy peaks were observed at, 779 cm^{-1}, 1026 cm^{-1}, 1154 cm^{-1}, 1294 cm^{-1}, 1448 cm^{-1}, 1535 cm^{-1}, 1629 cm^{-1}, 1872 cm^{-1}, 2336 cm^{-1}, 2844 cm^{-1}, 2919 cm^{-1} and 3114 cm^{-1}, which have PPy, and CA as shown in Fig. 1(c). The 779 cm^{-1}, 1026 cm^{-1}, 1154 cm^{-1}, 1294 cm^{-1}, 1448 cm^{-1}, 1535 cm^{-1}, 1629 cm^{-1} showed sharp intense peaks shifted position due to the presence of PPy which is coated on CA (Samancı et al., 2021; Hebalkar et al., 2005).

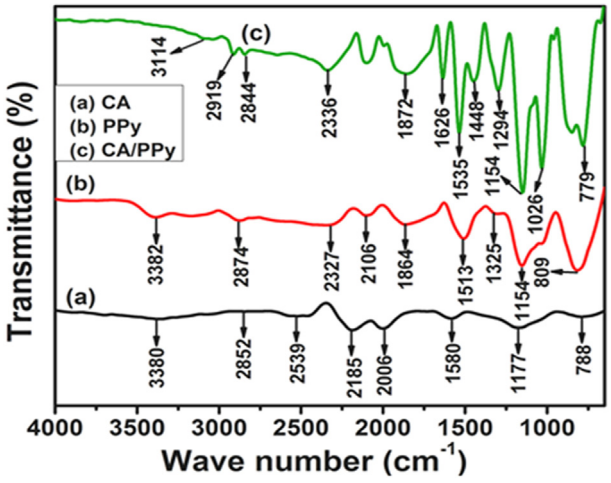

Fig. 1 (a): FTIR profile of CA (carbon aerogel). (b): FTIR profile of PPy (polypyrrole). (c): FTIR profile of CA/PPy (carbon aerogel and polypyrrole composite).

The polypyrrole showed C—H wagging at 808 cm^{-1} and 911 cm^{-1} to confirm the presence of an extended carbon structure. C$=$N, C—N, and N—H stretching vibrations were seen at 1680 cm^{-1}, 1317 cm^{-1} and 3550 cm^{-1}, respectively. Carbon to carbon double bonds were also seen at 1555 cm^{-1} and 1487 cm^{-1} to confirm the successful synthesis of polypyrrole. The spectrum of the CA-PPy composite the O—H, band was absent, a reduction in C—H stretch was observed and it also show the absence of some C—H bends. This indicates a successful binding of the functional sites of the CA and that of the PPy. Although, C$=$O, C—O, C—N bends remained visible on the FTIR spectrum for the CA-PPy composite at 1380 cm^{-1}, 1020 cm^{-1} and 1005 cm^{-1}, respectively.

4.2. XRD characterisation

XRD characterisation was used to evaluate the crystal nature of the as-prepared materials CA, PPy and CA-PPy composite, as shown in Fig. 2(a-c). On the diffraction pattern of CA, two peaks were observed at 22.42° and 43.79°, which were assigned to the (0 0 2) and (1 0 1) planes. These peaks are due to the graphite nature of CA as shown in Fig. 2(a) (Farma et al., 2013; Xu et al., 2017). Fig. 2(b) shows the diffraction pattern of PPy, a broad peak at 23.82° is observed which corresponded to the (0 0 2) plane, and it confirm the amorphous nature of PPy (Li et al., 2019b). Fig. 2(c) is the pattern of CA-PPy, it shows a less intense peak at 24.47° due to the graphitic properties of CA in the CA-PPy composite material. Other planes disappeared, suggesting the presence of a mixed structural form of the CA-PPy (Samancı et al., 2021).

4.3. Raman characterisation

Raman spectroscopy was also employed to investigate the materials' molecular structure, as shown in Fig. 3 The CA showed D and G bands at 1405 cm^{-1} and 1605 cm^{-1}. In addition, the 2G band was absent in the aerogel, but it shows the 2D band at 2410 cm^{-1}. The D band represents disorder and defects present in carbon after preparation, while the G band represents the carbon stretches in the benzene rings. The carbon aerogel, D and G bands were seen at 1408 cm^{-1} and 1609 cm^{-1} (Lim et al., 2013; Skrzypek, 2021). The significant difference between the carbon aerogel and the ordinary aerogel

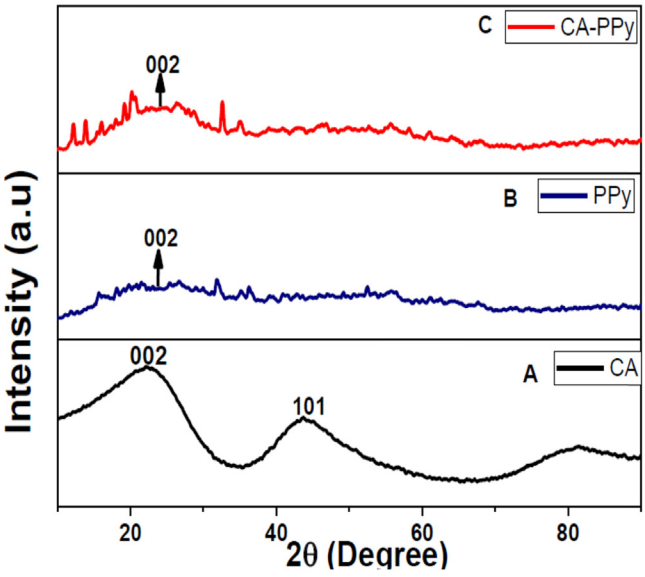

Fig. 2 (a): XRD profile of CA (carbon aerogel). (b): XRD profile of PPy (polypyrrole). (c): XRD profile of CA/PPy (carbon aerogel and polypyrrole composite).

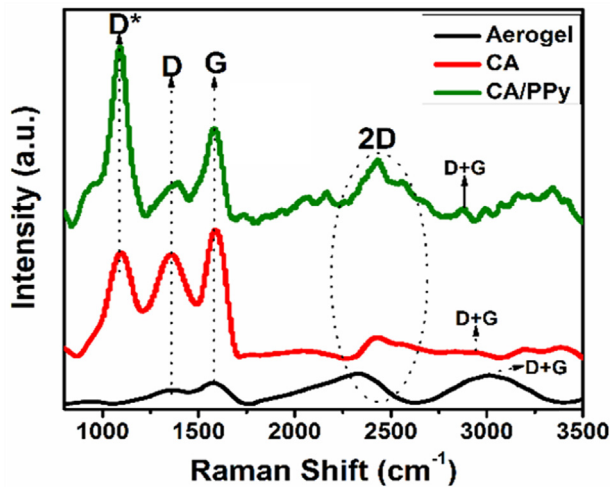

Fig. 3 (a): Raman spectroscopy of CA (carbon aerogel). (b): Raman spectroscopy of PPy (polypyrrole). (c): Raman spectroscopy of CA/PPy (carbon aerogel and polypyrrole composite).

is the 2G band at 1180 cm^{-1} in the carbon aerogel to confirm stacked sp^2 and sp^3 carbons in its ordered structure (Skrzypek, 2021).

In addition, the 2D band of the CA shifted forward to 2470 cm^{-1}; this is higher than that at 2410 cm^{-1} seen in the CA. The CA/PPy composite showed its D band at 1411 cm^{-1} and G band at 1610 cm^{-1}. Its 2G and 2D bands were seen at 1181 cm^{-1} and 2474 $cm^{-1,}$ respectively (Samancı et al., 2021; Xu et al., 2017; Lim et al., 2013; Skrzypek, 2021). The I_d/I_g was additionally calculated to reflect the graphitisation level in the carbon aerogel. Before the carbonisation of the aerogel, the I_d/I_g ratio was 0.63. After carbonisation, the carbon aerogel showed a I_d/I_g ratio of 0.74, showing a higher degree of graphitisation in the carbon aerogel (Lim et al., 2013).

4.4. BET characterisation

The materials' surface area and porosity measurements were determined by N_2 adsorption/desorption isotherm. Fig. 4(a and b) show the isotherms of the CA-PPy composite material. According to Fig. 4(a) the CA-PPy composite typically shows an IUPAC Type IV isotherm with a H3 hysteresis loop. The N_2 adsorption at low pressure indicates that the material contains a mixture of mesopores and macropores. The BET measurement of the surface area of the CA-PPy composite material is 496 m^2g^{-1} with an average pore diameter of 3.9 nm. The Barrett-Joyner-Halenda (BJH) analysis of the material's pore size is shown in Fig. 4(b). It shows the hierarchical porosity of CA-PPy composite material and large mesopore distribution. The large specific surface area and mesoporous texture indicate that the as-prepared CA-PPy composite material possesses proper morphology suitable as electrode material in hybrid CDI cells.

4.5. TGA characterisation

TGA was applied to study the thermal properties of CA, PPy, and CA-PPy. The thermograms of these materials are given in Fig. 5. The TGA analysis was conducted at 25 – 1000 °C and a heating rate of 10 °C/min. The CA showed thermal stability up to about 450 °C; at this temperature, a weight loss of 3 % was observed. Between 450 and 650 °C, the CA was significantly decomposed, and a mass loss of 97 % was recorded. The CA showed a two-step decomposition profile. The PPy and CA-PPy composite show similar thermal behaviour of a 3 % mass loss from 0 to 100 °C. They both exhibited a multi-step decomposition profile. The decomposition steps of the PPy are 3,10, 27, 9, and 3 %. A total of 52 % weight loss was recorded for the PPy, while that of the CA-PPy composite is 3,13, 22, 10, and 24 %. The PPy decomposed between 100 and 600 °C while the CA-PPy composite was at 100–700 °C. This data shows that the addition of the CA to the PPy slightly increased the thermal stability of the composite material and reduced the decomposition's starting temperature.

4.6. TEM characterisation

The microstructures of CA and CA-PPy were studied from TEM images. Fig. 6(A-F) shows the TEM images. The CA (Fig. 6A and B) images show a disorderly structure with the presence of cavities. The polypyrrole (C and D) images show that the PPy has a more orderly spherical form. The CA-PPy composite images (E and F) shows a mixed structure distribution with cavities. The presence of the cavities in the structure of the CA-PPy composite material provides sites for ion intercalation in hybrid CDI operations (Cao et al., 2019b; Zhuo et al., 2019).

4.7. SEM and EDAX characterisation

The microstructure of the materials was further investigated by SEM. The SEM images show a three-dimensional interconnected network of carbon aerogel flakes. The SEM images of the materials are shown in the Fig. 7(A-F). The EDAX spectrum of CA-PPy is displayed in Fig. 7G **(insert)**. The carbon

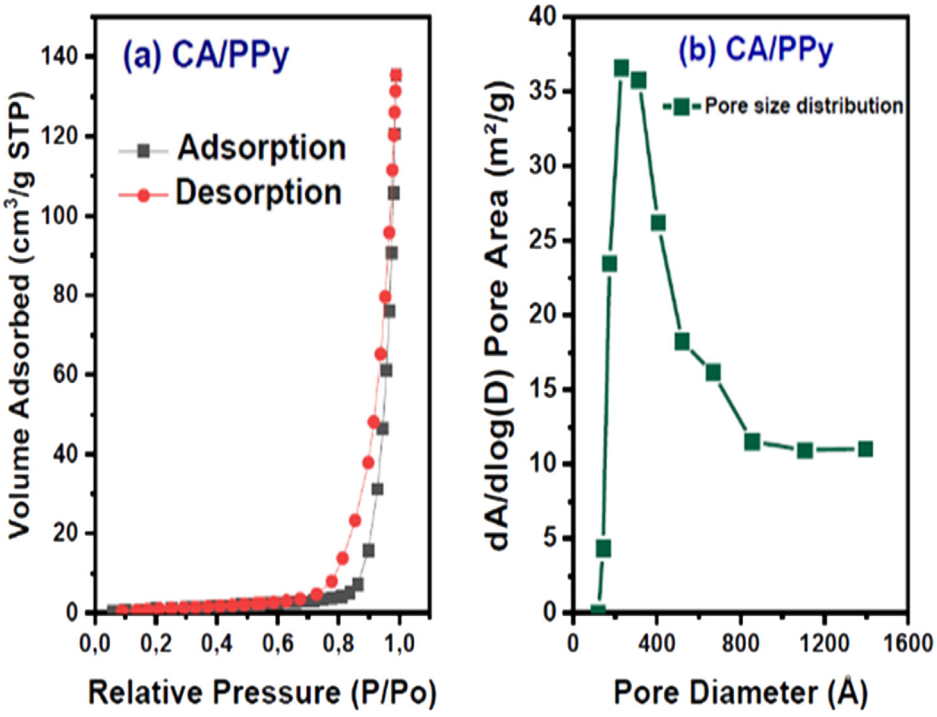

Fig. 4 (a): BET isotherm of CA- PPy (carbon aerogel and polypyrrole composite). (b): BJH Profile of pore size distribution of CA/PPy (carbon aerogel and polypyrrole composite).

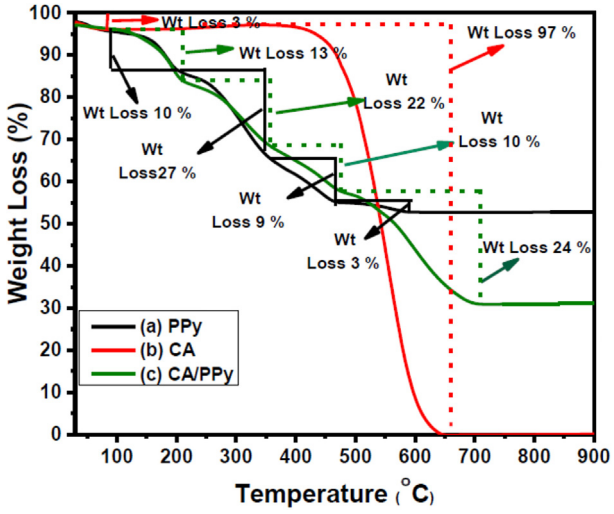

Fig. 5 (a): Thermogram of CA (b): Thermogram of PPy (c): Thermogram of CA/PPy.

aerogels exist in different sizes with smooth surfaces, as seen in Fig. 8(A and B). The SEM images of Polypyrrole (Fig. 7C and D) shows a foam-like structure. Fig. 7(E and F) shows the SEM images of CA-PPy composite. The surface of the CA-PPy composite is rough compared to that of CA in Fig. 7(A and B); this suggests that the PPy is successfully coated on the CA in the CA-PPy composite.

EDAX analysis was also employed to determine the elemental composition of the CA-PPy composite. The EDAX result of the CA-PPy composite is shown in Fig. 7G (**insert**). The chlorine in the material as reflected in the EDAX spectrum is most likely from the $FeCl_3$ oxidant used in the synthesis of the PPy.

4.8. CV and EIS tests of materials

The electrochemical properties of the materials were determined by cyclic voltammetry (CV) and electrochemical impedance spectroscopy (EIS). The materials' CV profiles and Nyquist plots are shown in Figs. 8 and 9, respectively. The CV profile of CA, Fig. 8(a) and CA-PPy, Fig. 8(b) confirms that reversible reactions take place for the two samples. The smooth polygonal shape (without distinct anodic and cathodic peaks) of CA Fig. 8(a) shows its capacitive nature (Rambabu et al., 2020). In the CA-PPy CV profile, Fig. 8(b), the curves showing the anodic and cathodic current peaks are distinct and imply the presence of Faradaic current. This is indicative of the pseudo-capacitive property of the CA-PPy composite. The specific capacitance of the CA-PPy composite at 5 mV/s scan rate is 360.1F/g. This value agrees with that reported by Zhou H et al. 345F/g for CA-PPy. The specific capacitance of the CA at 5 mV/s is 115F/g. The increase in capacitance of the CA-PPy composite confirms that the addition of PPy to the CA improves its capacitance in the composite. The PPy is a battery material that has been reported to have a high energy density, hence it is used as a component of supercapacitors (Samancı et al., 2021; Kim et al., 2012). This supports the ability of PPy to enhance the capacitance of CA in the composite material. It also suggests that the CA/PPy composite material undergoes redox reactions resulting in pseudocapacitance (Samancı et al., 2021).

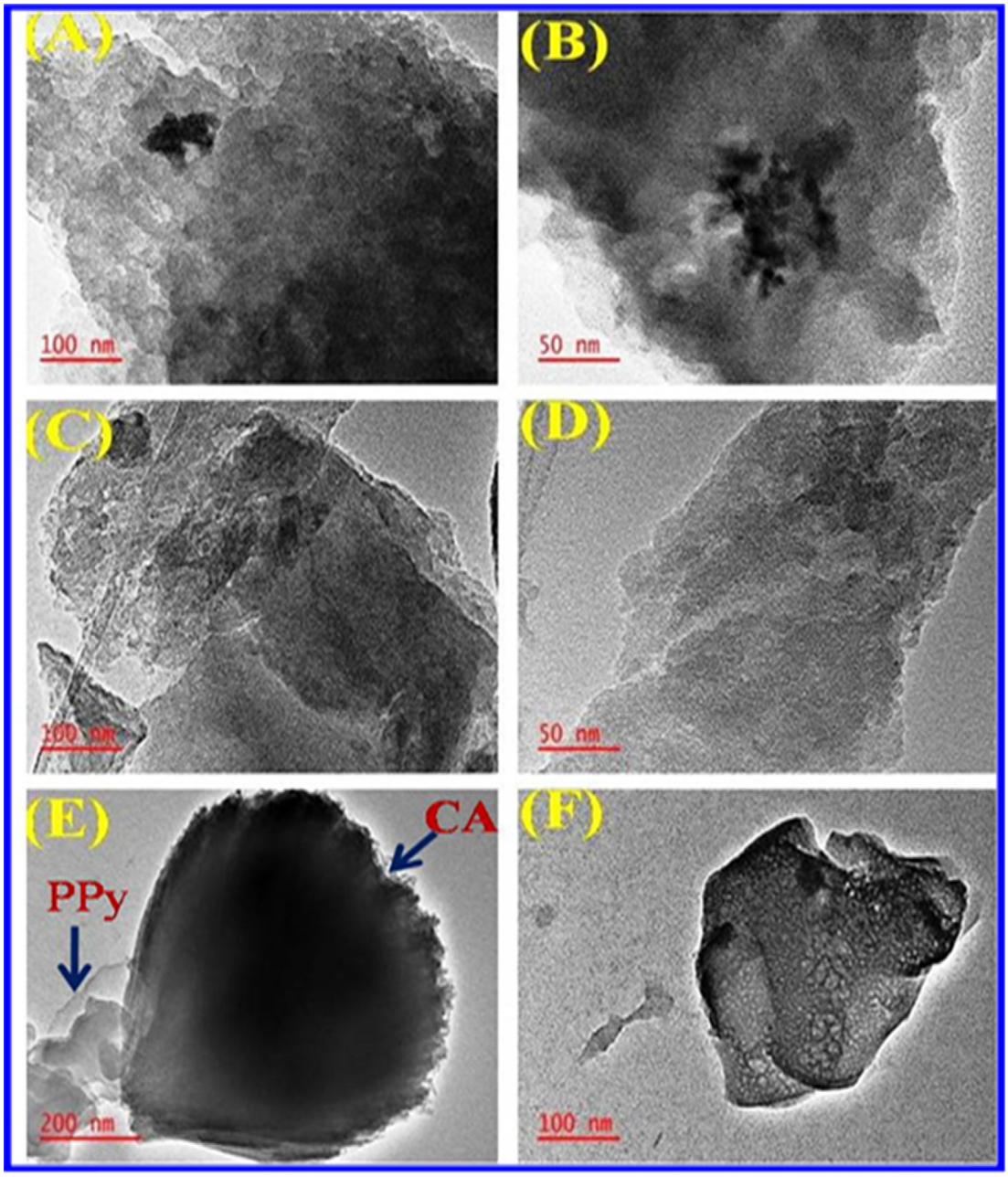

Fig. 6 (a – b): TEM images of CA. (c – d): TEM images of PPy (e – f): TEM images of CA/PPy.

The CV profiles of the CA-PPy composite at different scan rates are also shown in Fig. 9. When the scan rate is increased to 50 mV/s, the shape of the voltammogram remains polygonal, with the cathodic and anodic current peaks intact. This means that an increase in the scan rate will not necessarily affect the ion adsorption/desorption mechanism at the electrical double layer of the electrode/electrolyte interface.

Fig. 10 shows the profile of the specific capacitance of the CA-PPy composite at different scan rates. A decrease in specific capacitance was observed at higher scan rates. At 5 mV/s, the specific capacitance is 360.1F/g and at 50 mV/s the scan rate decreased to 280.3F/g. The observation agrees with reports of similar research (Rambabu et al., 2020). The decrease in specific capacitance can be attributed to the insufficient time for ion diffusion into the gaps and inner pores of the CA-PPy composite electrode. The ion adsorption and desorption rates are slow at lower scan rates, and there isn't sufficient time for ion diffusion. Hence the specific capacitance value is higher at lower scan rates.

The electrochemical properties of the CA and CA-PPy composite were further investigated by EIS. The EIS studies were conducted at a potential of 0.22 V and a frequency range of 10^5 Hz to 0.1 Hz. Fig. 11 shows the Nyquist plots of CA and CA-PPy. At a high frequency, the impedance acted as resistance, but as the frequency decreased, the impedance increased. The impedance line is about 45° to the imaginary axis, typical of porous electrode materials; it also confirms the dependence of the ions in the saline solution on frequency

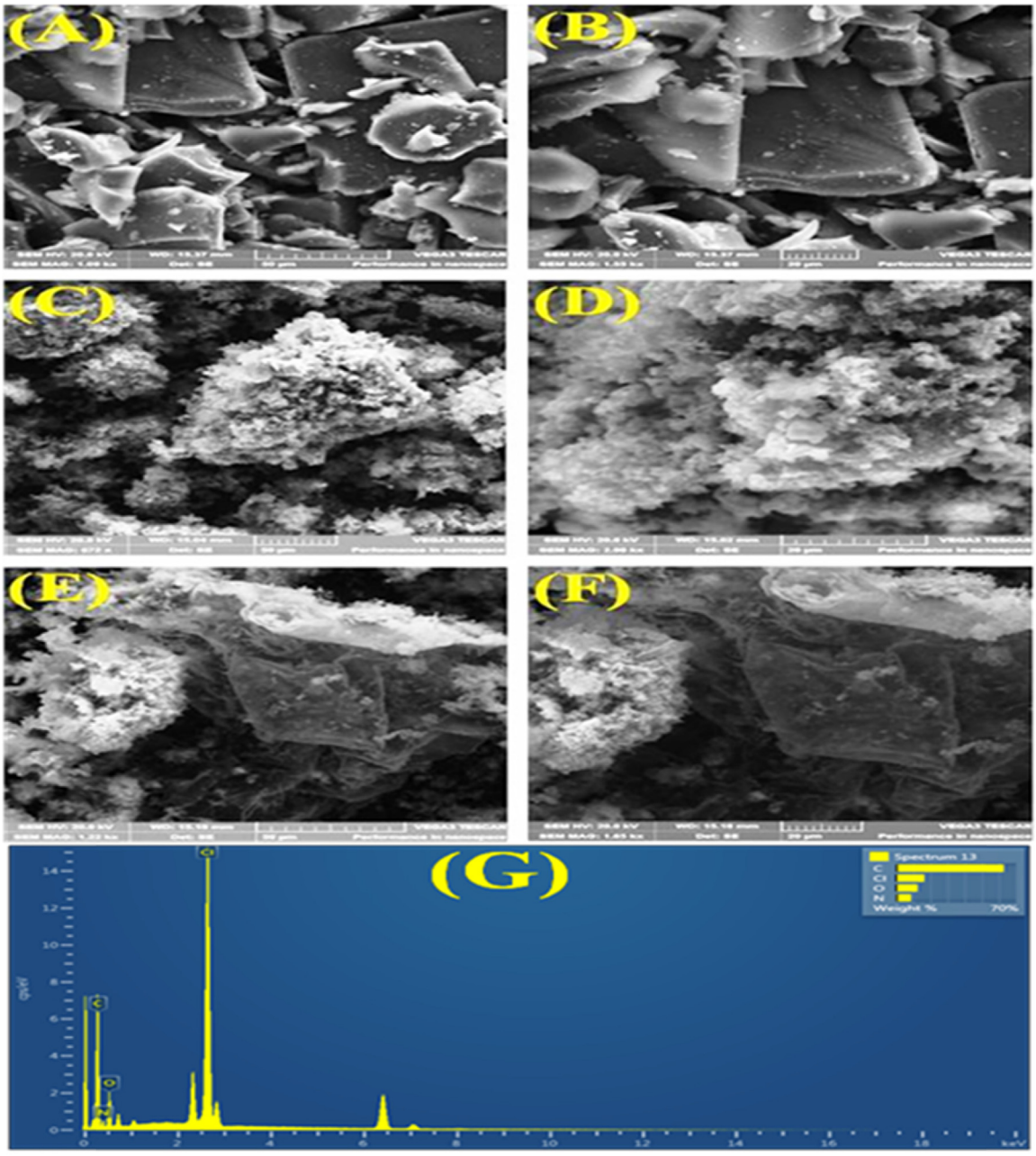

Fig. 7 (a – b): SEM images of CA. (c – d): SEM images of PPy. (e – f): SEM images of CA/PPy. (G – G[1]): EDAX spectra showing the elemental composition of CA/PPy.

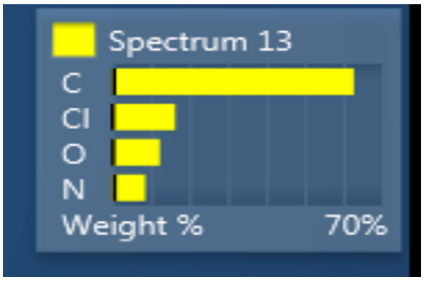

Fig. 7 (*continued*)

(Kandalkar et al., 2011). The charge transfer resistances were found to be 240 Ω for the CA sample, and 170 Ω for the CA-PPy composite. The CA-PPy composite depicted a smaller semi-circle than CA due to the improved charge transfer of electrons due to the presence of PPy. PPy is a known efficient electrical conductor due to its pi-pi delocalised bonds (Bose et al., 2011; Kulandaivalu et al., 2019). Therefore, the CA-PPy composite has a better charge transfer which could benefit ion transport, leading to an enhanced salt removal rate.

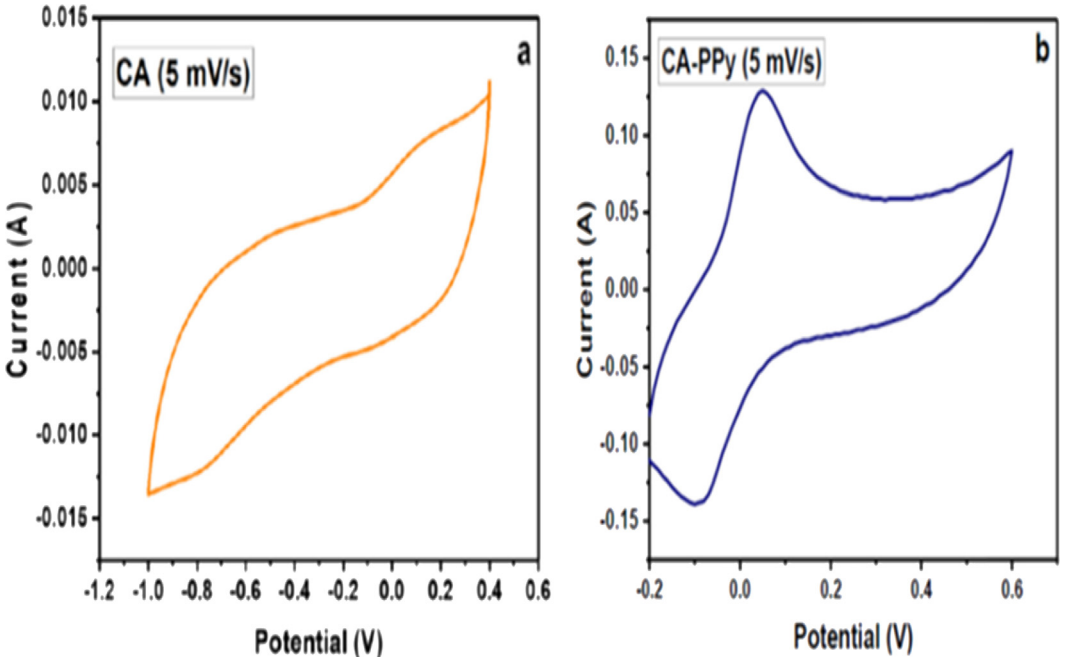

Fig. 8 (a): CV Profile of CA at 5 mV/s scan rate. (b): CV profile of CA/PPy at 5 mV/s scan rate.

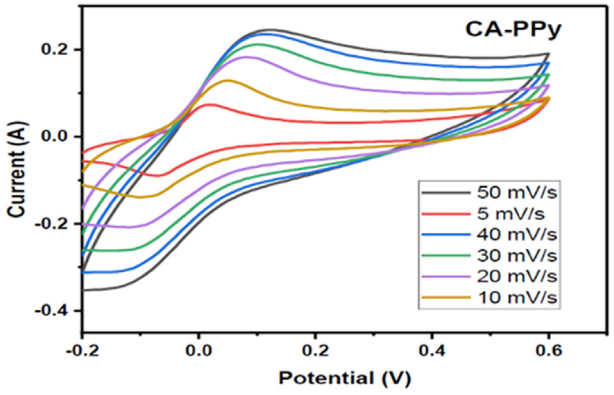

Fig. 9 CV of CA/PPy at different scan rates.

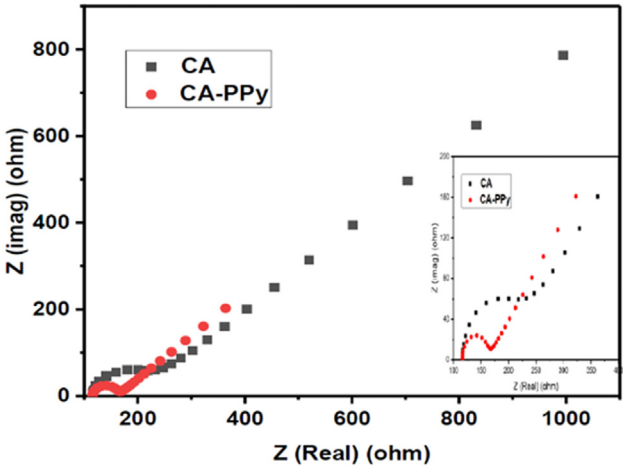

Fig. 11 Nyquist plots of CA and CA-PPy at 50 mV/s scan rate.

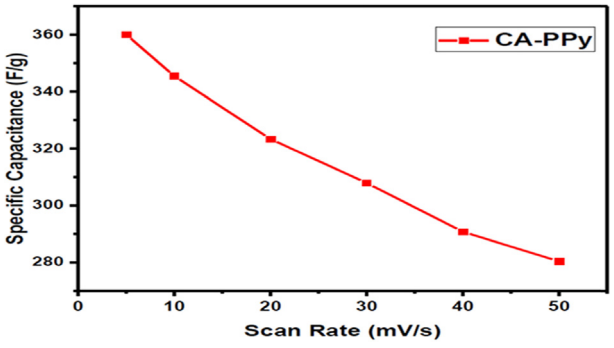

Fig. 10 Profile of the specific capacitance of CA-PPy at different scan rates.

4.9. CDI desalination study

The CDI removal of Na^+ and Cl^- by the CA-PPy composite was done by a batch mode experiment. Three different concentrations of saline solutions (300 mg/L, 500 mg/L, and 800 mg/L) were used, and the applied potential was 1.2 V. The anode was a 0.5 cm by 1.0 cm activated carbon modified with CA-PPy composite, while the cathode was a 0.5 cm by 1.0 cm activated carbon sheet. A 50 mL saline solution was transferred into a 100 mL beaker containing the two electrodes and a conductivity meter. The electrodes were then connected to a DC source. When the potential was applied, Na^+ and Cl^- migrated to the anode and cathode, respectively. The experiment proceeded until the electrodes were saturated with the ions. The conductivity of the solution was monitored and recorded at

intervals by the conductivity meter throughout the investigation. The saline solution was continually stirred with a magnetic stirrer to prevent the accumulation of charges in a particular region of the cell. The experimental setup is shown in Scheme 3.

On application of the potential, the conductivity of the solution dropped quickly for a while. A steady decline was observed until it became stable for about an hour, indicating ion adsorption saturation at the electrodes.

The experiment was repeated several times to evaluate the stability and ion retention capacity of the CA-PPy composite electrode after cycles of ion adsorption /desorption.

Fig. 12 (a) shows the profile of SAC vs Time for the different concentrations of NaCl solutions, while Fig. 12(b) shows that of the conductivity of NaCl solutions against time. Fig. 12(a) shows a sharp rise in SAC on applying the potential; this gradually reduces until saturation is reached. In Fig. 12(b), the conductivity of the NaCl solution decreases as ion adsorp-

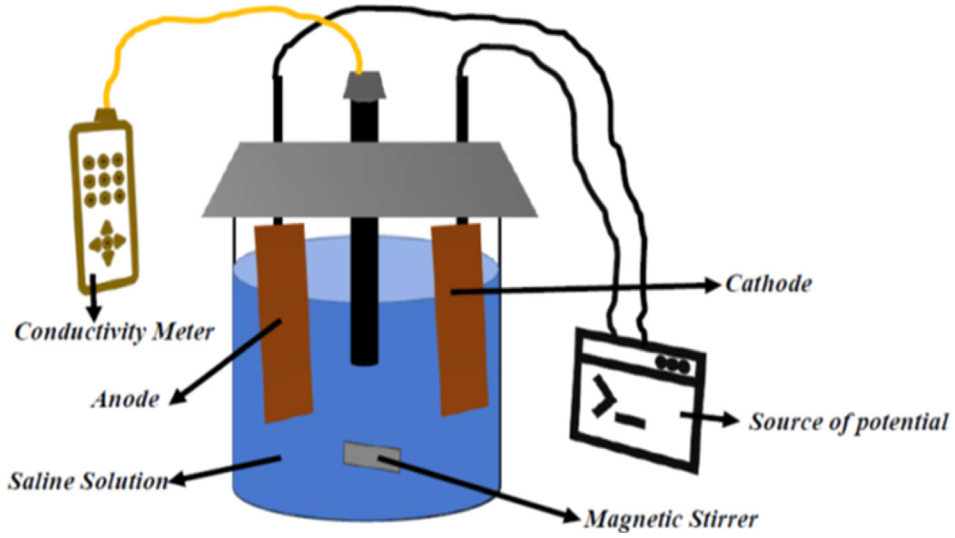

Scheme 3 Schematic of hybrid CDI desalination experimental set-up.

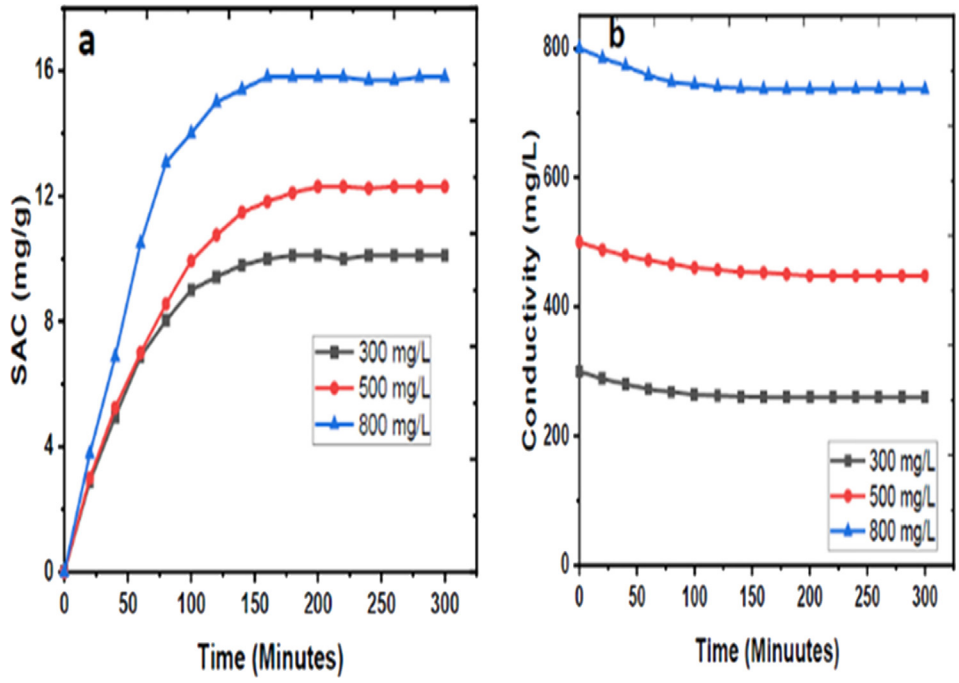

Fig. 12 (a) Graph of SAC vs Time. (b) Graph of Conductivity vs Time for the different concentrations.

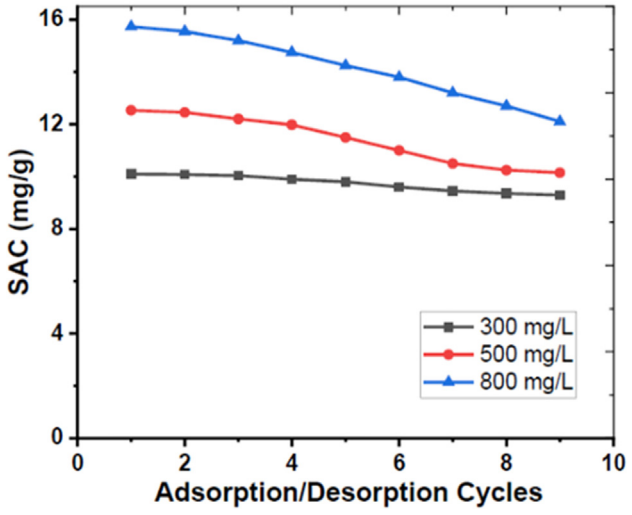

Fig. 13 Graph of SAC vs Ion Adsorption/Desorption Cycles.

tion proceeds. The salt recovery efficiency of the electrode material at the different concentrations of saline solutions was also determined from their conductivity values using Eq. (3) as displayed in Section 3.2.

The electrochemical stability and ion retention capacity of the CA-PPy composite were evaluated by a study of several ion adsorption/desorption cycles. Fig. 13 shows the profile of the SAC and ion retention capacity after nine cycles of ion adsorption/desorption of (300, 500, and 800) mg/L of NaCl solutions.

The SAC and ion retention values decrease gradually for each cycle, as shown in Table 1. This indicates the CA-PPy is an electrochemically stable electrode material. Table 2 compares the SAC and electrochemical properties of our material and that of similar materials that have been previously reported. The results indicate that the CA-PPy composite is a decent material for application in CDI desalination.

5. Conclusion and recommendations

The CA-PPy composite was successfully prepared, and its physical and electrochemical properties were investigated using different analytical instruments. The composite material was then used to modify activated carbon electrodes. It was then applied for the desalination of (300, 500, and 800) mg/L NaCl solutions by the hybrid CDI method. From the study, the CA-PPy composite electrode recorded (10.1, 12.53, and 15.7) mg/g ion adsorption capacity and an SRE (%) of (27, 20.12, and 15.41) for the (300, 500, and 800) mg/L NaCl solutions respectively at an applied potential of 1.2 V. This show that the electrode material is most efficient at lower concentrations of solutions. It also has a specific capacitance of 360.1F/g at a scan rate of 5 mV/s in a 1.0 M KCl solution. At higher scan rates a decrease in Cs was observed. After nine cycles of ion adsorption/desorption study, the CA-PPy composite shows good electrochemical stability with ion retention capacities of 92 %, 81 %, and 77 % in the (300, 500, and 800) mg/L NaCl solutions, respectively. The results recorded show that the prepared electrode material has a good ion adsorption capacity and electrochemical stability for desalination by the hybrid capacity deionisation method, with better salt removal in solutions with lower concentrations.

6. Recommendations

The following recommendations are made for future studies.

1. The effects of pH and Temperature on salt removal capacity should be considered
2. The effect of improved porosity of the CA by heating it to about 1000 °C should be considered.

Funding

This work was funded by the Faculty of Science, the University of Johannesburg., NRF Thuthuka grant and Dr Nimbofa. (The sources of funding listed did not contribute

Table 1 Showing SAC, and ion retention values after nine cycle of ion adsorption/desorption.

Concentrations (mg/L)	SAC after First Cycle (mg/g)	SAC after Nineth Cycle (mg/g)	Ion retention Capacity
300	10.1	9.29	92 %
500	12.53	10.15	81 %
800	15.73	12.1	77 %

Table 2 Comparison of the CDI results of CA/PPy and CDI results of other electrode materials.

Serial Number	Electrode Material	Specific Capacitance (F/g)	Initial Concentration (mg/L)	Applied Voltage (V)	Desalination capacity (mg/g)	Reference
1	CA	141	100	1.2	5.27	(Cao et al., 2019b)
2	Graphene composite CA	————	500	1.2	26.9	(Zhang et al., 2019)
3	CA	262	800	1.2	10.54	(Kumar et al., 2016)
4	Graphene bonded CA	220	500	1.2	15.7	(Luo et al., 2017)
5	CA-PPy	360.1	800	1.2	15.7	Current Study

to the manuscript writing, and they did not make any input for the manuscript submission).

Declaration of Competing Interest

The authors declare that they have no known competing financial interests or personal relationships that could have appeared to influence the work reported in this paper.

References

Alaei Shahmirzadi, M.A., Hosseini, S.S., Luo, J., Ortiz, I., 2018. Significance, evolution and recent advances in adsorption technology, materials and processes for desalination, water softening and salt removal. J. Environ. Manage. 215, 324–344. https://doi.org/10.1016/j.jenvman.2018.03.040.

Al-Karaghouli, A., Kazmerski, L.L., 2013. Energy consumption and water production cost of conventional and renewable-energy-powered desalination processes. Renew. Sustainable Energy Rev. 24, 343–356. https://doi.org/10.1016/j.rser.2012.12.064.

Al-Muhtaseb, S.A., Ritter, J.A., 2003. Preparation and properties of resorcinol–formaldehyde organic and carbon gels. Adv. Mater. 15, 101–114. https://doi.org/10.1002/adma.200390020.

Bose, S., Kim, N.H., Kuila, T., Lau, K.T., Lee, J.H., 2011. Electrochemical performance of a graphene-polypyrrole nanocomposite as a supercapacitor electrode. Nanotechnology. 22. https://doi.org/10.1088/0957-4484/22/29/295202.

Buczek, S., Barsoum, M.L., Uzun, S., Kurra, N., Andris, R., Pomerantseva, E., Mahmoud, K.A., Gogotsi, Y., 2020. Rational design of titanium carbide MXene electrode architectures for hybrid capacitive deionization. Energy Environ. Mater. 3, 398–404. https://doi.org/10.1002/eem2.12110.

Burn, S., Hoang, M., Zarzo, D., Olewniak, F., Campos, E., Bolto, B., Barron, O., 2015. Desalination techniques - A review of the opportunities for desalination in agriculture. Desalination 364, 2–16. https://doi.org/10.1016/j.desal.2015.01.041.

Cao, J., Wang, Y., Wang, L., Yu, F., Ma, J., 2019a. Na(3)V(2)(PO(4))(3)@C as faradaic electrodes in capacitive deionization for high-performance desalination. Nano Lett. 19, 823–828. https://doi.org/10.1021/acs.nanolett.8b04006.

Cao, Z., Zhang, C., Yang, Z., Qin, Q., Zhang, Z., Wang, X., Shen, J., 2019b. Preparation of carbon aerogel electrode for electrosorption of copper ions in aqueous solution. Materials 12. https://doi.org/10.3390/ma12111864.

Chen, P.A., Cheng, H.C., Wang, H.P., 2018. Activated carbon recycled from bitter-tea and palm shell wastes for capacitive desalination of salt water. J Clean Prod. 174, 927–932. https://doi.org/10.1016/j.jclepro.2017.11.034.

Cheng, Y., Hao, Z., Hao, C., Deng, Y., Li, X., Li, K., Zhao, Y., 2019. A review of modification of carbon electrode material in capacitive deionization. RSC Adv. 9, 24401–24419. https://doi.org/10.1039/c9ra04426d.

Chitte, H.K., Shinde, G.N., Bhat, N.V., Walunj, V.E., 2011. Synthesis of polypyrrole using ferric chloride ($FeCl_3$) as oxidant together with some dopants for use in gas sensors. J Sens Technol. 01, 47–56. https://doi.org/10.4236/jst.2011.12007.

Choi, J.H., 2014. Determination of the electrode potential causing Faradaic reactions in membrane capacitive deionization. Desalination. 347, 224–229. https://doi.org/10.1016/j.desal.2014.06.004.

Duan, F., Du, X., Li, Y., Cao, H., Zhang, Y., 2015. Desalination stability of capacitive deionization using ordered mesoporous carbon: effect of oxygen-containing surface groups and pore properties. Desalination. https://doi.org/10.1016/j.desal.2015.08.009.

Fahmida, P., Sultana, A., 2018. Desalination technologies for developing countries: a review. J. Sci. Res.

Farma, R., Deraman, M., Awitdrus, I.A., Talib, R., Omar, J.G., Manjunatha, M.M., Ishak, N.H., Basri, B.N.M.D., 2013. Physical and electrochemical properties of supercapacitor electrodes derived from carbon nanotube and biomass carbon. Int. J. Electrochem. Sci. 8, 257–273.

Haro, M., Rasines, G., MacIas, C., Ania, C.O., 2011. Stability of a carbon gel electrode when used for the electro-assisted removal of ions from brackish water. Carbon N Y. 49, 3723–3730. https://doi.org/10.1016/J.CARBON.2011.05.001.

Hebalkar, N., Arabale, G., Sainkar, S.R., Pradhan, S.D., Mulla, I.S., Vijayamohanan, K., Ayyub, P., Kulkarni, S.K., 2005. Study of correlation of structural and surface properties with electrochemical behaviour in carbon aerogels. J Mater Sci. 40, 3777–3782. https://doi.org/10.1007/s10853-005-3318-4.

Elsayed, M.A., Hall, P.J., Heslop, M.J., 2007. Preparation and structure characterization of carbons prepared from resorcinol-formaldehyde resin by CO_2 activation Preparation and structure characterization of carbons prepared from resorcinol-formaldehyde resin by CO_2 activation. https://doi.org/10.1007/s10450-007-9065-x.

Hu, P., Tan, B., Long, M., 2016. Advanced nanoarchitectures of carbon aerogels for multifunctional environmental applications. Nanotechnol Rev. 5, 23–39. https://doi.org/10.1515/ntrev-2015-0050.

Jia, B., Zhang, W., 2016. Preparation and application of electrodes in Capacitive Deionization (CDI): a state-of-art review. Nanoscale Res Lett. 11, 1–25. https://doi.org/10.1186/s11671-016-1284-1.

Kandalkar, S.G., Lee, H.M., Chae, H., Kim, C.K., 2011. Structural, morphological, and electrical characteristics of the electrodeposited cobalt oxide electrode for supercapacitor applications. Mater Res Bull. 46, 48–51. https://doi.org/10.1016/j.materresbull.2010.09.041.

Khawaji, A.D., Kutubkhanah, I.K., Wie, J.M., 2008. Advances in seawater desalination technologies. Desalination 221, 47–69. https://doi.org/10.1016/j.desal.2007.01.067.

Kim, S.Y., Hong, J., Palmore, G.T.R., 2012. Polypyrrole decorated cellulose for energy storage applications. Synth Met. 162, 1478–1481. https://doi.org/10.1016/j.synthmet.2012.06.003.

Kobayashi, A., Konishi, G.I., 2009. Synthesis and analysis of resorcinol-acetone copolymer. Molecules 14, 364–377. https://doi.org/10.3390/molecules14010364.

Kulandaivalu, S., Suhaimi, N., Sulaiman, Y., 2019. unveiling high specific energy supercapacitor from layer-by-layer assembled polypyrrole/graphene oxide|polypyrrole/manganese oxide electrode material. Sci. Rep. 9. https://doi.org/10.1038/s41598-019-41203-3.

Kumar, N.A., Choi, H.J., Shin, Y.R., Chang, D.W., Dai, L., Baek, J. B., 2012. Polyaniline-grafted reduced graphene oxide for efficient electrochemical supercapacitors. ACS Nano. 6, 1715–1723. https://doi.org/10.1021/NN204688C.

Kumar, R., Sen Gupta, S., Katiyar, S., Raman, V.K., Varigala, S.K., Pradeep, T., Sharma, A., 2016. Carbon aerogels through organo-inorganic co-assembly and their application in water desalination by capacitive deionization. Carbon N Y. 99, 375–383. https://doi.org/10.1016/j.carbon.2015.12.004.

Laxman, K., Myint, M.T.Z., Al Abri, M., Al-Gharibi, L., Al Namani, B., Bourdoucen, H., Dutta, J., 2015. Efficient desalination of brackish ground water via a novel capacitive deionization cell using nanoporous activated carbon cloth electrodes. J. Eng. Res. 12, 22–31. https://doi.org/10.24200/tjer.vol12iss2pp22-31.

Li, S., Chen, Y., He, X., Mao, X., Zhou, Y., Xu, J., Yang, Y., 2019a. Modifying reduced graphene oxide by conducting polymer through a hydrothermal polymerization method and its application as energy storage electrodes. Nanoscale Res.

Li, F., Xiea, L., Suna, G., Konga, Q., Sua, F., Caoc, Y., Weia, J., Ahmada, A., Guod, X., Chena, C.-M., 2019b. Resorcinol-formaldehyde based carbon aerogel: Preparation, structure and

applications in energy storage devices. Micropor. Mesopor. Mat. 279, 293–315. https://doi.org/10.1016/j.micromeso.2018.12.007.

Li, J., Cheng, X., Shashurin, A., Keidar, M., 2012. Review of electrochemical capacitors based on carbon nanotubes and graphene. Graphene. 01, 1–13. https://doi.org/10.4236/graphene.2012.11001.

Li, B., Jiang, S., Yu, S., Chen, Y., Tang, X., Wu, X., Zhong, Y., Shen, X., Cui, S., 2018. Co-polyimide aerogel using aromatic monomers and aliphatic monomers as mixing diamines. J. Solgel Sci. Technol. 88, 386–394. https://doi.org/10.1007/s10971-018-4800-1.

Lim, Y.S., Tan, Y.P., Lim, H.N., Huang, N.M., Tan, W.T., 2013. Preparation and characterization of polypyrrole/graphene nanocomposite films and their electrochemical performance. J. Polymer Res. https://doi.org/10.1007/s10965-013-0156-y.

Liu, P., Yan, T., Shi, L., Park, H.S., Chen, X., Zhao, Z., Zhang, D., 2017. Graphene-based materials for capacitive deionization. J. Mater. Chem. A. 5, 13907–13943.

Luo, G., Wang, Y., Gao, L., Zhang, D., Lin, T., 2017. Graphene bonded carbon nanofiber aerogels with high capacitive deionization capability. Electrochim. Acta 260, 656–663. https://doi.org/10.1016/j.electacta.2017.12.012.

Mahani, A.A., Motahari, S., Nayyeri, V., 2018. Electromagnetic and microwave absorption characteristics of PMMA composites filled with a nanoporous resorcinol formaldehyde based carbon aerogel. RSC Adv. 8, 10855–10864. https://doi.org/10.1039/c8ra00196k.

Meena, A.K., Mishra, G.K., Rai, P.K., Rajagopal, C., Nagar, P.N., 2005. Removal of heavy metal ions from aqueous solutions using carbon aerogel as an adsorbent. J. Hazard Mater. 122, 161–170. https://doi.org/10.1016/J.JHAZMAT.2005.03.024.

Oh, H.J., Lee, J.H., Ahn, H.J., Jeong, Y., Kim, Y.J., Chi, C.S., 2006. Nanoporous activated carbon cloth for capacitive deionization of aqueous solution. Thin Solid Films 515, 220–225. https://doi.org/10.1016/j.tsf.2005.12.146.

Oh, H., Lee, J., Ahn, H., Jeong, Y., Kim, Y., Chi, C., 2006. Nanoporous activated carbon cloth for capacitive deionization of aqueous solution. Thin Solid Films 515, 220–225. https://doi.org/10.1016/j.tsf.2005.12.146.

Oladunni, J., Zain, J.H., Hai, A., Banat, F., Bharath, G., Alhseinat, E., 2018. A comprehensive review on recently developed carbon based nanocomposites for capacitive deionization: from theory to practice. Sep Purif Technol. 207, 291–320. https://doi.org/10.1016/j.seppur.2018.06.046.

Oyarzun, D.I., Hemmatifar, A., Palko, J.W., Stadermann, M., Santiago, J.G., 2018. Ion selectivity in capacitive deionization with functionalized electrode: theory and experimental validation. Water Res X. 1, 1–10. https://doi.org/10.1016/j.wroa.2018.100008.

Pekala, R.W., 1989. Organic aerogels from the polycondensation of resorcinol with formaldehyde. J. Mater. Sci. 24, 3221–3227. https://doi.org/10.1007/BF01139044.

Pera-Titus, M., Yamauchi, Y., Yonar, T., Yang, T., Xu, X., Lin, P., Liao, M., Sheng, X., Wu, Y., 2020. Modification of metal-organic framework-derived nanocarbons for enhanced capacitive deionization performance: a mini-review. Front. Chem. | Www Frontiersin. Org. 1,. https://doi.org/10.3389/fchem.2020.575350 575350.

Porada, S., Zhao, R., van der Wal, A., Presser, V., Biesheuvel, P.M., 2013. Review on the science and technology of water desalination by capacitive deionization. Prog. Mater. Sci. 58, 1388–1442. https://doi.org/10.1016/j.pmatsci.2013.03.005.

Qin, M., Deshmukh, A., Epsztein, R., Patel, S.K., Owoseni, O.M., Walker, W.S., Elimelech, M., 2019. Comparison of energy consumption in desalination by capacitive deionization and reverse osmosis. Desalination 455, 100–114. https://doi.org/10.1016/j.desal.2019.01.003.

Rambabu, K., Bharath, G., Hai, A., Luo, S., Liao, K., Haija, M.A., Banat, F., Naushad, M., 2020. Development of watermelon rind derived activated carbon/manganese ferrite nanocomposite for cleaner desalination by capacitive deionization. J Clean Prod. 272. https://doi.org/10.1016/j.jclepro.2020.122626.

Razaq, A., Nyholm, L., Sjödin, M., Strømme, M., Mihranyan, A., 2012. Paper-based energy-storage devices comprising carbon fiber-reinforced polypyrrole-cladophora nanocellulose Composite electrodes. Adv. Energy Mater. 2, 445–454. https://doi.org/10.1002/AENM.201100713.

Ryoo, M., Kim, J., Seo, G., 2003. Role of titania incorporated on activated carbon cloth for capacitive deionization of NaCl solution. J. Colloid Interface Sci. 264, 414–419. https://doi.org/10.1016/S0021-9797(03)00375-8.

Samancı, M., Daş, E., Bayrakçeken Yurtcan, A., 2021. Carbon aerogel and their polypyrrole composites used as capacitive materials. Int J Energy Res. 45, 1729–1747. https://doi.org/10.1002/er.5841.

Skrzypek, E., 2021. First- and second-order Raman spectra of carbonaceous material through successive contact and regional metamorphic events (Ryoke belt, SW Japan). Lithos 388–389. https://doi.org/10.1016/j.lithos.2021.106029.

Tan, N.P.B., Ucab, P.M.L., Dadol, G.C., Jabile, L.M., Talili, I.N., Cabaraban, M.T.I., 2022. A review of desalination technologies and its impact in the Philippines. Desalination. 534. https://doi.org/10.1016/j.desal.2022.115805.

Tannert, R., Schwan, M., Ratke, L., n.d., Reduction of shrinkage and brittleness for resorcinol-formaldehyde aerogels by means of a pH-controlled sol-gel process.

Torres Hernández, W., 2018. An electrochemical desalination cell based on conducting polymers. Revista de Ciencias. 21, 101. https://doi.org/10.25100/rc.v21i1.6344.

Volfkovich, Y.M., 2020. Capacitive deionization of water (a review). Russian J. Electrochem. 56, 18–51. https://doi.org/10.1134/S1023193520010097.

Wang, H., Hao, Q., Yang, X., Lu, L., Wang, X., 2010. Effect of graphene oxide on the properties of its composite with polyaniline. ACS Appl Mater Interfaces. 2, 821–828. https://doi.org/10.1021/AM900815K.

Wang, Y., Wang, R., Xu, S., Liu, Q., Wang, J., 2015. Polypyrrole/polyaniline composites with enhanced performance for capacitive deionization. Desalination Water Treat. 54, 3248–3256. https://doi.org/10.1080/19443994.2014.907748.

Wang, H., Xu, E., Yu, S., Li, D., Quan, J., Xu, L., Wang, L., Jiang, Y., 2018. Reduced graphene oxide-anchored manganese hexacyanoferrate with low interstitial H_2O for superior sodium-ion batteries. ACS Appl. Mater. Interfaces 10, 34222–34229. https://doi.org/10.1021/acsami.8b11157.

Xia, L., Zhang, M., Rong, M., Guo, K., Hu, Y., Wu, Y., Czigany, T., 2012. An easy soft-template route to synthesis of wormhole-like mesoporous tungsten carbide/carbon composites. Compos. Sci. Technol. 72, 1651–1655. https://doi.org/10.1016/J.COMPSCITECH.2012.07.007.

Xu, Y., Sui, Z., Xu, B., Duan, H., Zhang, X., 2012. Emulsion template synthesis of all conducting polymer aerogels with superb adsorption capacity and enhanced electrochemical capacitance. J. Mater. Chem. 22, 8579–8584. https://doi.org/10.1039/c2jm30565h.

Xu, Y., Yan, M., Wang, S., Zhang, L., Liu, H., Liu, Z., 2017. Synthesis, characterization and electrochemical properties of carbon aerogels using different organic acids as polymerization catalysts. J. Porous Mater. 24, 1375–1381. https://doi.org/10.1007/s10934-017-0379-0.

Yang, J., Zou, L., Song, H., 2011. Preparing MnO_2/PSS/CNTs composite electrodes by layer-by-layer deposition of MnO_2 in the membrane capacitive deionisation. Desalination. https://doi.org/10.1016/j.desal.2011.11.013.

Yong-Jin Han, T., Worsley, M.A., Baumann, T.F., Satcher, J.H., 2011. Synthesis of ZnO coated activated carbon aerogel by simple sol-gel route. J. Mater. Chem. 21, 330–333. https://doi.org/10.1039/c0jm03204b.

Zhang, C., Wang, X., Wang, H., Xueling, W., Shen, J., 2019. Ambient Pressure-Dried Graphene-Composite Carbon Aerogel for Capacitive Deionization. Process 7, 29. https://doi.org/10.3390/pr7010029.

Zhang, W., Mossad, M., Zou, L., 2013. A study of the long-term operation of capacitive deionisation in inland brackish water desalination. Desalination. 320, 80–85. https://doi.org/10.1016/j.desal.2013.04.010.

Zhang, H., Wang, J., Shan, Q., Wang, Z., Wang, S., 2013. Tunable electrode morphology used for high performance supercapacitor: polypyrrole nanomaterials as model materials. Electrochim Acta. 90, 535–541. https://doi.org/10.1016/J.ELECTACTA.2012.12.045.

Zhao, S., Yan, T., Wang, Z., Zhang, J., Shi, L., Zhang, D., 2017. Removal of NaCl from saltwater solutions using micro/mesoporous carbon sheets derived from watermelon peel via deionization capacitors. RSC Adv. 7, 4297–4305. https://doi.org/10.1039/c6ra27127h.

Zhuo, H., Hu, Y., Chen, Z., Zhong, L., 2019. Cellulose carbon aerogel/PPy composites for high-performance supercapacitor. Carbohydr. Polym. 215, 322–329.